Coriolis and ultrasonic flow meters in phase-contaminated oil flows

Dennis van Putten, René Bahlmann (DNV GL)

DNV GL Oil & Gas
Energieweg 17, 9743 AN Groningen
dennis.vanputten@dnvgl.com

1 INTRODUCTION

Oil and gas operators today are facing several significant measurement challenges in their efforts to optimize production and generate more from their reservoirs. One main challenge is how to deal with the measurement of multiphase flows. The application of multiphase flow meters (MPFM's) has increased significantly over the last decades to overcome this challenge. These MPFM's have in principle the capability of covering the entire multiphase flow regime, but may not be the best choice when considering costs and accuracy in specific regions of the multiphase flow domain.

Many oil fields nowadays are producing small levels of phase-contamination (i.e. small volume fractions of water and gas). This may be caused by using enhanced oil recovery techniques or due to the production towards the end-of-life of a field. These phase-contaminations are typically small compared to the main flow and therefore single phase measurements with appropriate compensation methods might be used. In many situations, an MPFM may not be fit-for-purpose and the single-phase flow meter might outperform the MPFM in terms of accuracy and costs. For these applications, an uncertainty of approximately 5-10% is typically allowed which aids in the successful application of single phase flow meters.

Single phase flow meters are often installed in situations where under normal operation a pure oil stream is expected, e.g. downstream of a separator, at custody transfer locations or at bunkering stations. The transported fluids are often near their bubble point and may partially evaporate due to changes in process conditions. The phase equilibrium by itself is very sensitive and calculations require accurate input data, like upstream process conditions and composition of the fluids, to predict the onset of degassing.

The impact on the introduction of a second phase should be well understood since it can lead to relative high biases due to the non-linear behaviour of a multiphase flow. These systematic errors enter the allocation process and can lead to large financial risk. For phase-contaminated oil flows both over-readings and under-readings of a single-phase flow meter are possible, since the type of contamination and its physical behaviour determine the interaction with the continuous phase. Also, different metering technology respond differently to the introduction of contamination.

DNV GL has executed a Joint Testing Project (JTP) with a large E&P and Coriolis and ultrasonic flow meter manufacturers. The project aimed to set up testing guidelines, evaluate the performance of the flow meters and to understand the over/under-reading behaviour of these flow meters in phase-contaminated oil flow. Tests with different meter designs of 4" and 6" size were carried out under oil flow conditions and subjected to water and gas contamination within the limits $0 \leq \mathrm{WLR} \leq 1$ and $\mathrm{GVF} < 0.1$. In Figure 1-1, an example of a two-phase flow regime map is depicted. For phase-

contaminated oil flow, the flow regimes that are typically encountered are stratified flow, elongated bubble flow and dispersed bubble flow.

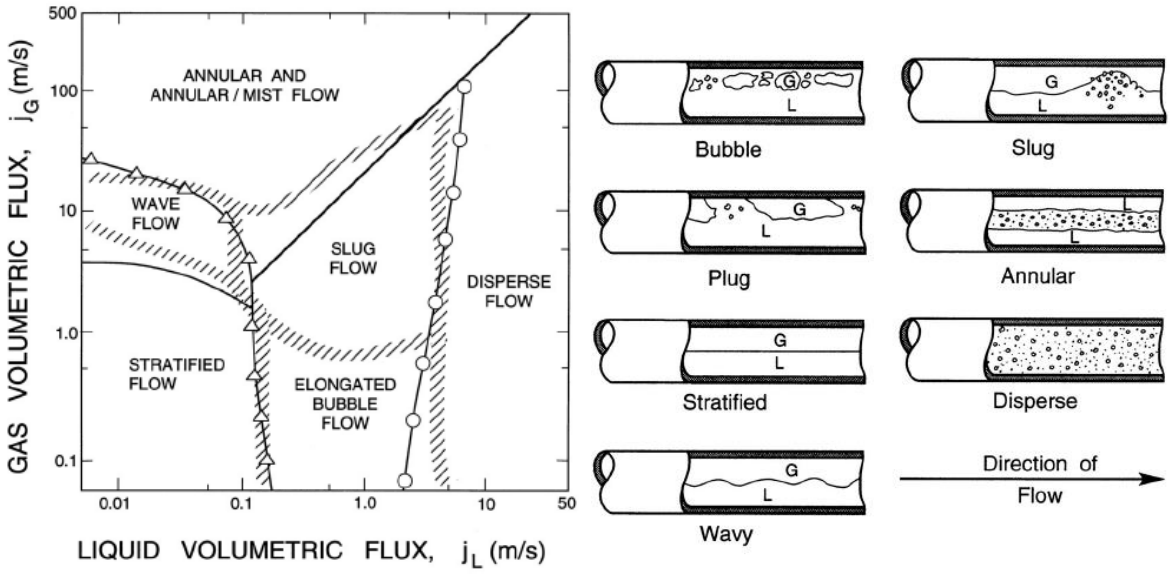

Figure 1-1 : Flow regime map for atmospheric air/water mixtures in horizontal configuration as a function of the phase volumetric flux (left) and corresponding flow patterns (right), with L and G denoting liquid and gas, respectively (figures from ref [2]).

It was observed that the complexity of a multiphase flow and the size of the parameters space are greatly reduced by using dimensional analysis in which the behaviour (e.g. flow regime and gas bubble size) is expressed in terms of dimensionless numbers, e.g. Froude number and Reynolds number. This approach was already successfully applied by DNV GL in wet gas environments for ultrasonic meters [9] and explored by several manufacturers in phase-contaminated liquid flows [11].

2 FUNDAMENTAL MULTIPHASE FLOW PHYSICS

Before presenting the test results it is necessary to perform a fundamental analysis of the fluid dynamical equations of a multiphase fluid. This analysis will provide the dominant parameters that will govern the behavior of the multi-phase flow, i.e. the flow regime and the gas hold-up, and therefore the response of the single-phase flow meters. First, the two-phase liquid-gas system is discussed where the liquid is assumed homogeneous and the gas fraction is assumed small. In the second part of this section the flow regimes and their transition of a two-phase oil-water flow are discussed.

2.1 Fluid dynamical equations of two-phase liquid dominated flow

At this stage, we consider a steady state two-phase gas-liquid system and will assume the oil-water mixture to be fully mixed and revert to this assumption in the final part of this section. The mixture rules for the physical properties are based on a homogeneous mixture assumption, see e.g. [9].

Also, we will assume the differential pressure to be negligible, which is a common assumption for (nearly) full bore geometries, like ultrasonic flow meters. The differential pressure of Coriolis meters

may be substantial at high flow rates; however, the occurrence of these high differential pressure conditions was minimized in the JTP tests. Also, this analysis provides the upstream flow regimes and does not consider the flow regime alteration induced by the internal geometry of the flow meters or by the unsteady conditions generated by the flow meter, e.g. the tube frequency of a Coriolis meter.

Starting from the local instant formulation [5], the Navier-Stokes equations for phase *k* in absence of differential pressure is given by

$$\nabla \cdot \left(\rho_k \mathbf{u}_k \mathbf{u}_k \right) = \nabla \cdot \tau_k + \rho_k \mathbf{g} \qquad \textbf{(1)}$$

where subscript *k* is either the gas phase (*g*), the oil phase (*o*), the water phase (*w)* or the combined liquid phase (*l*). The phase density is given by ρ_k, the phase velocity vector by $\mathbf{u}_k$, the phase stress tensor by τ_k and $\mathbf{g}$ the gravitational acceleration vector. The interface conditions for the conservation of mass results in the equality of the velocity vectors at the interface: $\mathbf{u}_g = \mathbf{u}_l$. The interface condition for the momentum balance is given by

$$\left(\tau_l - \tau_g \right) \cdot \mathbf{n}_g = \gamma_{l/g} \kappa \mathbf{n}_g \qquad \textbf{(2)}$$

where the unit outward normal of the gas-liquid interface and is denoted by $\mathbf{n}_g$, $\gamma_{l/g}$ is the gas-liquid surface tension and $\kappa = \nabla \cdot \mathbf{n}_g$ is the surface curvature.

Using an appropriate (constant) reference state (indicated by superscript *), all physical quantities can be written in dimensionless form (indicated by a tilde); i.e. $a_k = a_k^* \tilde{a}_k$. For liquid dominant pipe flow with diameter D, the scaling of both the liquid and gas phase equation is done by $\rho_l^* u_l^{*2} / D$; where ρ_l^* and u_l^* are the reference density and velocity of the liquid phase, respectively. Applying this scaling to all equations leads to the dimensionless form of the Navier-Stokes equations

$$\begin{aligned} \mathrm{X}_{\mathrm{LM},l(g)}^2 \tilde{\nabla} \cdot \left(\tilde{\rho}_g \tilde{\mathbf{u}}_g \tilde{\mathbf{u}}_g \right) &= \frac{\mathrm{X}_{\mathrm{LM},l(g)}^2}{\mathrm{Re}_g} \tilde{\nabla} \cdot \tilde{\tau}_g + \frac{\mathrm{DR}_{l(g)}}{\hat{\mathrm{Fr}}_l^2} \mathbf{e}_z \\ \tilde{\nabla} \cdot \left(\tilde{\rho}_l \tilde{\mathbf{u}}_l \tilde{\mathbf{u}}_l \right) &= \frac{1}{\mathrm{Re}_l} \tilde{\nabla} \cdot \tilde{\tau}_l + \frac{1}{\hat{\mathrm{Fr}}_l^2} \mathbf{e}_z \end{aligned} \qquad \textbf{(3)}$$

where Re_k is the *k* phase Reynolds number, $\mathrm{X}_{\mathrm{LM},l(g)}$ is the inverse of the Lockhart-Martinelli parameter as defined in wet gas (which is denoted by $\mathrm{X}_{\mathrm{LM},g(l)}$), $\hat{\mathrm{Fr}}_l$ is the liquid Froude number and $\mathrm{DR}_{l(g)}$ is the gas-liquid density ratio:

$$\mathrm{Re}_k = \frac{\rho_k u_{sk} D}{\mu_k} \tag{4}$$

$$\hat{\mathrm{Fr}}_l = \frac{u_{sl}}{\sqrt{gD}}$$

$$\mathrm{X}_{\mathrm{LM},l(g)} = \sqrt{\frac{\rho_g}{\rho_l}}\frac{u_{sg}}{u_{sl}} = \mathrm{X}^{-1}_{\mathrm{LM},g(l)}$$

$$\mathrm{DR}_{l(g)} = \frac{\rho_g}{\rho_l}$$

and $\mathbf{e}_z$ is the unit vector in z-direction. The subscript notation, $l(g)$, denotes liquid as the continuous/dominant phase and the gas as the dispersed/submissive phase. For the experiments in this study, the liquids and gases can be assumed incompressible and therefore the reference states of the densities and viscosities are taken as $\rho_k^* = \rho_k$ and $\mu_k^* = \mu_k$. For the reference velocities, the superficial velocities are used: $u_k^* = u_{sk}$.

From the interface condition in equation **(2)**, we obtain one additional dimensionless number; the liquid Weber number

$$\mathrm{We}_{l(g/l)} = \frac{\rho_l u_{sl}^2 D}{\gamma_{g/l}} \tag{5}$$

For convenience, the liquid densiometric Froude number, $\mathrm{Fr}_{l(g)}$, is defined, in which the density ratio is considered in the buoyancy term, resulting in

$$\mathrm{Fr}_{l(g)} = \frac{u_{sl}}{\sqrt{gD}}\sqrt{\frac{\rho_l}{\rho_l - \rho_g}} \approx \hat{\mathrm{Fr}}_l \tag{6}$$

For the typical conditions in gaseous liquid flow these Froude numbers are approximately equal. Also, typically the gas can be considered inviscid so that the dependence on the gas Reynolds number can be neglected.

So, for liquid dominant flow with small fractions of gas, the multiphase dynamics is determined by the group of dimensionless numbers

$$\mathrm{Re}_l,\ \mathrm{Fr}_{l(g)},\ \mathrm{X}_{\mathrm{LM},l(g)},\ \mathrm{We}_{l(g/l)},\ \mathrm{DR}_{l(g)}. \tag{7}$$

The main contributors to the dynamics are expected to be the $\mathrm{X}_{\mathrm{LM},l(g)}$, which is proportional to the gas volume fraction and the $\mathrm{Fr}_{l(g)}$ and $\mathrm{We}_{l(g/l)}$, which will dominate the flow regime transition.

In the current derivation, the liquid mixture is assumed homogeneously mixed. To prove this, a similar analysis can be performed for the oil-water mixture resulting in the group of dimensionless numbers

$$\mathrm{Re}_w,\ \mathrm{Re}_o,\ \hat{\mathrm{Fr}}_l,\ \mathrm{WLR},\ \mathrm{We}_{l(w/o)},\ \mathrm{DR}_{l(w)}. \tag{8}$$

Where the parameters can be interpreted in the same way as for the gas-liquid flow. The WLR is the water liquid ratio which determines the continuous liquid phase; the $\hat{\mathrm{Fr}}_l$ and $\mathrm{We}_{l(w/o)}$ (and to some extent the oil Reynolds number) determine the flow regime transition. The additional dimensionless numbers are:

$$\mathrm{WLR} = \frac{u_{sw}}{u_{sl}} \tag{9}$$

$$\mathrm{DR}_{l(k)} = \frac{\rho_k}{\rho_l}$$

$$\mathrm{We}_{l(w/o)} = \frac{\rho_l u_{sl}^2 D}{\gamma_{w/o}}$$

It is noted that the oil-liquid density ratio, $\mathrm{DR}_{l(o)}$, can be derived from the $\mathrm{DR}_{l(w)}$ and the WLR.

2.2 Gas-liquid flow regime transition in liquid dominated flow

Weisman [12] improved the Taitel-Dukler model [10] by including diameter and surface tension effects and based the transition model on a large set of experimental data. The original expression presented by Weisman on the transition to fully dispersed flow can be rewritten in terms of dimensionless numbers

$$\mathrm{Fr}^*_{l(g)} = 0.3\mathrm{Eo}^{-\frac{1}{4}}_{l(g)}\,\mathrm{Re}^{\frac{1}{2}}_l \qquad (\text{laminar}) \tag{10}$$

$$\mathrm{Fr}^*_{l(g)} = 4.28\mathrm{Eo}^{-\frac{1}{4}}_{l(g)}\,\mathrm{Re}^{\frac{1}{8}}_l \qquad (\text{turbulent})$$

where $\mathrm{Eo}_{l(g)}$ is called the Eötvös number and is defined as

$$\mathrm{Eo}_{l(g)} \equiv \frac{\mathrm{We}_{l(g)}}{\mathrm{Fr}^2_{l(g)}} = \frac{(\rho_l - \rho_g)gD^2}{\gamma_{g/l}} \tag{11}$$

Typical values for the critical liquid Froude number for the dispersed transition point in a 6” pipe are: 1.5 (oil/gas) and 2.8 (water/gas) and for the 4” pipe: 2.0 (oil/gas) and 3.6 (water/gas).

Also, a model is presented to estimate the transition between stratified and intermittent plug flow, which can be simplified to: $\mathrm{Fr}^*_{l(g)} \approx 0.25$.

It is emphasized that a “transition point” does not exist and typically the multiphase flow topology transits gradually between designated flow regimes. Therefore, the provided numbers should be considered as indicative values.

The dimensionless numbers that appear in these models where derived in equation **(7)** and it seems that the total amount of injected gas and the pressure do not significantly alter the transition point, i.e.

no dependence on $X_{LM,l(g)}$ and $DR_{l(g)}$. The data from Weisman [12] confirm the expectation that the $Fr_{l(g)}$ and $We_{l(g/l)}$ dominate this transition process.

2.3 Oil-water flow regime transition

Typical values for the transition between stratified and dispersed oil-water flow are of the order of $u_{sl} \approx 1-2$ m/s for small diameter pipes, see e.g. refs [1] and [4] as well as Figure 2-1. It is expected that this condition should be converted to a condition in terms of dimensionless numbers, i.e. in terms of $\hat{Fr}_l$. Combining the overview of experimental data from Elseth [4] and Angeli [1], a Froude number condition can be constructed

$$\hat{Fr}_l^* = 2.4 \quad \textbf{(12)}$$

which results in approximately $u_{sl} = 2.4$ m/s for a 4" line and $u_{sl} = 2.9$ m/s for a 6" line. Again, it is noted that a transition point does not exist and the transition from stratified to dispersed flow for an oil-water mixture is a gradual transition. The transition from a purely stratified flow to a partly mixed flow already occurs at typically a third of the critical Froude number given in equation **(12)**, i.e. $\hat{Fr}_l^* \approx 0.8$. Another interesting phenomenon is the phase inversion point, denoted by WLR^*, i.e. the point at which the flow transits from oil-continuous flow with water droplet to water-continuous flow with oil droplets. This point is indicated in Figure 2-1 by the vertical solid lines. For the Exxsol D120 oil used during the JTP test, this inversion point is at $WLR^* \approx 0.3$.

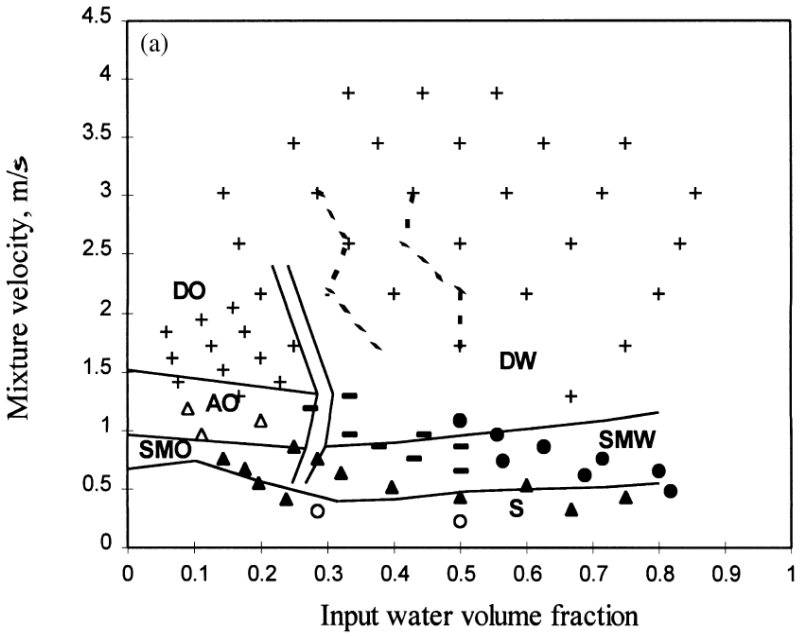

Figure 2-1 : Oil-water flow pattern map for a 1 inch pipe as a function of superficial liquid velocity and WLR (S=stratified, SMO=stratified mixed and oil, SMW=stratified mixed and water, DO=dispersed water in oil, DW=dispersed oil in water), taken from Angeli [1].

It is noted that in the discussion of the results in the next section, the $\mathrm{Fr}_{l(g)}$ is used for presentation of the oil-water results for consistency. This is allowed, since it was proven in equation **(6)** that $\mathrm{Fr}_{l(g)} \approx \hat{\mathrm{Fr}}_l$.

The test matrix is constructed so that all indicated flow regimes in this section are attained in the 4" test line with a liquid Froude number range between 0.5 and 5. In general, the 6" test line will have a higher number of test points in the stratified flow regime.

3 TEST EXECUTION

The test facility used in this JTP is the MultiPhase Flow Laboratory of DNV GL in Groningen. A general description of the facility including an explanation of the flow rate reconstruction and uncertainty model can be found in ref [8]. The facility performs well for oil dominant flow conditions and the uncertainties of the reference flow rates are within 1%.

The study is limited to the flow regimes in liquid dominated flows, i.e. $\mathrm{GVF} < 10\%$ and $0 \leq \mathrm{WLR} \leq 1$. The tests in the JTP are performed at pressures between 12 and 32 bara at an ambient temperature between 15 and 20°C. The fluids used are natural gas and argon for the gas phase; Exxsol D120 as the oil phase and salt water with a salinity of 4.6%wt.

3.1 Test matrix

The test matrix is constructed based on a horizontal 4" S80 test line. Test matrix focusses on covering the flow regimes discussed in the preceding section. This means that for the 6" line the distribution is less optimal and the meters are mainly tested in the stratified flow regimes. Although it was devised that the flow regimes and their transition are dominated by the dimensionless numbers (like liquid Froude number), the test matrix is defined in terms of the total liquid volume flow, Gas Volume Fraction (GVF) and Water Liquid Ratio (WLR).

- Pressure [bara]: [12, 14.5, 32]
- Temperature [°C]: [15-20]
- Flow rates:
  - Liquid flow rates: [**15, 30, 60**, 90, **120**, 150] m^3/h
  - GVF: [**0, 1, 2, 4, 6, 8**] %
  - WLR: [**0**, 5, **10, 25**, 30, 90, **100**] %
- Fluids:
  - Gas: Natural gas, Argon
  - Oil: Exxsol D120 (density [815-830] kg/m^3, viscosity ~4.8 cP)
  - Water: Salt water (salinity ~4.6wt%)

The gas phase was changed from natural gas to argon during the test. Argon is used to mimic high pressures (i.e. high density ratios) and to investigate the effect of inert versus dissolvable gas on the performance of the flow meters. In total, the test matrix consists of 389 test points and the bold numbers in the listed conditions are the core matrix.

4 TEST RESULTS

In this section the results are given for the two metering technologies, i.e. Coriolis and ultrasonic flow meters. The results will be presented anonymously and only the data is presented that was labelled valid by the manufacturer prior to receiving the reference results of the facility.

Before subjecting the flow meters to multiphase flow conditions, a baseline test was performed at pure oil and pure water flow to correct for any possible initial bias in the single-phase results. The first part of this section will discuss the results of the two technology groups in oil-water flow conditions. The second part will discuss the results for multiphase conditions. Each section is preceded by the fluid dynamical observations of the flow regimes.

4.1 Oil-water mixtures

A relative extensive test matrix is executed for analysis of the oil-water response of the flow meters. The entire WLR -range as described in section 3.1 is covered to provide detailed information on the use of Coriolis and ultrasonic flow meters in this specific application.

For the Coriolis mass flow meters, the relative error between the liquid mass flow rate of the Meter Under Test (MUT) and the reference liquid flow rate (*ref*) is defined as

$$\varepsilon_m = \frac{\dot{m}_l^{MUT} - \dot{m}_l^{ref}}{\dot{m}_l^{ref}}, \tag{13}$$

where $\dot{m}_l^{MUT}$ is the measured liquid mass flow rate by the MUT and $\dot{m}_l^{ref} = \dot{m}_w^{ref} + \dot{m}_o^{ref}$ is the actual liquid mass flow rate given by the reference system of the test facility, both at line conditions. For the ultrasonic flow meters, the relative error between the liquid volumetric flow rate of the Meter Under Test (*MUT*) and the reference liquid flow rate (*ref*) is defined as

$$\varepsilon_Q = \frac{Q_l^{MUT} - Q_l^{ref}}{Q_l^{ref}}, \tag{14}$$

where Q_l^{MUT} is the measured liquid volumetric flow rate by the MUT and Q_l^{ref} is the actual liquid volumetric flow rate given by the reference system of the test facility, both at line conditions.

4.1.1 Flow regimes

The observed flow regimes in the 4" line for several $\mathrm{Fr}_{l(g)}$ for $\mathrm{WLR} = 0.25$ are presented in Figure 4-1. It is again noted that the presentation of the results is done in terms of $\mathrm{Fr}_{l(g)}$ for consistency with the proceeding sections, while the use of $\hat{\mathrm{Fr}}_l$ would be physically more correct since no gas is present. The

difference between the values is however negligible for the conditions tested in this JTP, see equation **(6)**. The superficial velocity in a 4" line is approximately equal to the $\mathrm{Fr}_{l(g)}$-number and is given in the figure caption between brackets. The figure labels (a), (b) and (c) will be used in the subsequent figures to connect the $\mathrm{Fr}_{l(g)}$ dependence of the flow regime to the obtained measurement results.

Figure 4-1 (c) and (d) provide the result for a dispersed flow in the oil-continuous and water-continuous flow regime, respectively.

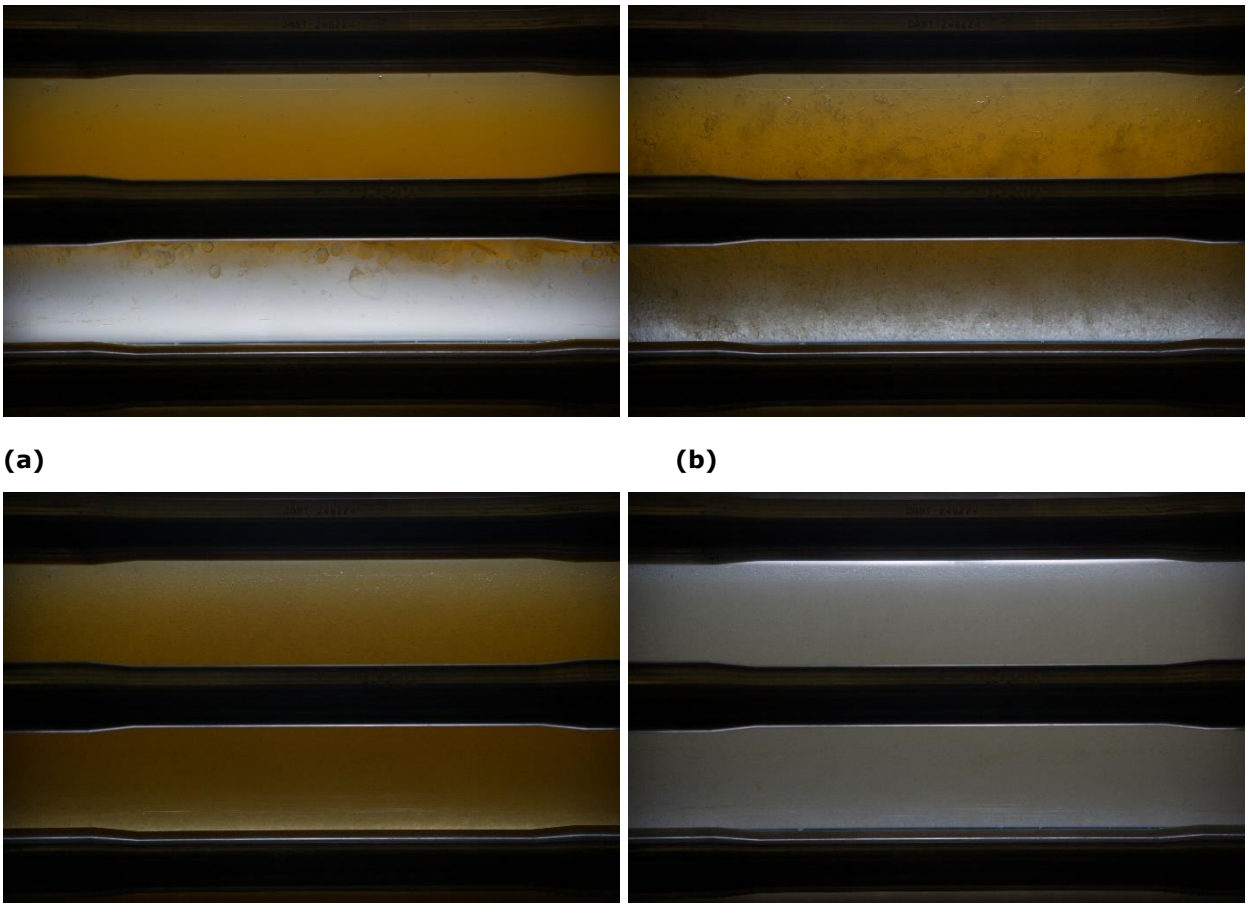

(a) **(b)**

(c) **(d)**

Figure 4-1 : Observed flow regimes for oil-water mixtures for: (a) $\mathrm{Fr}_{l(g)} = 1.2\ (u_{sl} = 1.1)$ **and** $\mathrm{WLR} = 0.3$**, (b)** $\mathrm{Fr}_{l(g)} = 2.3\ (u_{sl} = 2.3)$ **and** $\mathrm{WLR} = 0.3$**, (c)** $\mathrm{Fr}_{l(g)} = 3.5\ (u_{sl} = 3.4)$ **and** $\mathrm{WLR} = 0.05$ **(oil-continuous), (d)** $\mathrm{Fr}_{l(g)} = 3.5\ (u_{sl} = 3.4)$ **and** $\mathrm{WLR} = 0.9$ **(water-continuous)**

4.1.2 Coriolis meters

The Coriolis meters typically work under homogenous oil-water flow. The onset to mixed oil-water flow is at relative low Froude numbers and even at stratified conditions the meter should provide reasonable results due to the smaller internal diameter of the Coriolis tubes, i.e. increased local liquid Froude number.

The results of the total liquid mass flow error of the Coriolis meters as a function of WLR and $\mathrm{Fr}_{l(g)}$ are presented in Figure 4-2. As observed from Figure 4-2, the error stays within a few percent and increases with decreasing WLR. The latter effect can be a result of minor degassing of the oil phase and cannot be purely attributed to the Coriolis meters. The error decreased as the flow becomes more homogeneous, especially above $\mathrm{Fr}_{l(g)} = 2.5$, which is consistent with the theoretical predictions in section 2.3 and the observations in Figure 4-1 (b) and (c).

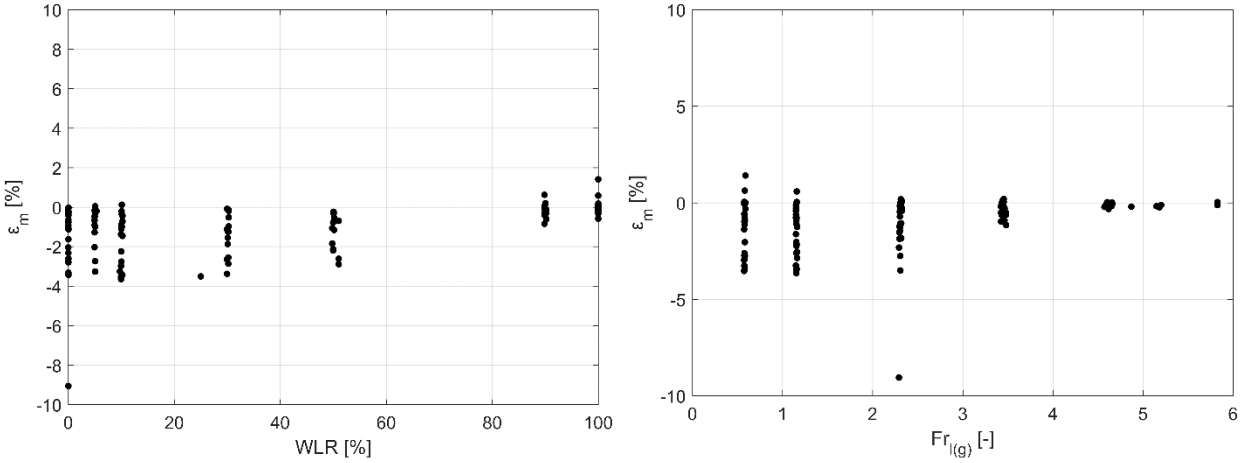

Figure 4-2 : Mass flow error for oil-water mixtures as a function WLR (left) and $\mathrm{Fr}_{l(g)}$ (right) for Coriolis meters

The measured density of the Coriolis meters is compared with the mixture density of the facility, assuming the mixture is homogeneous. As explained in the preceding section, this assumption is only valid for high liquid Froude numbers and at low Froude numbers slight slip between the oil and water may occur. The results of the density error as a function of WLR and $\mathrm{Fr}_{l(g)}$ are presented in Figure 4-3. The behaviour as a function of $\mathrm{Fr}_{l(g)}$ is very dominant and at high values the flow becomes more homogeneous and the error reduces.

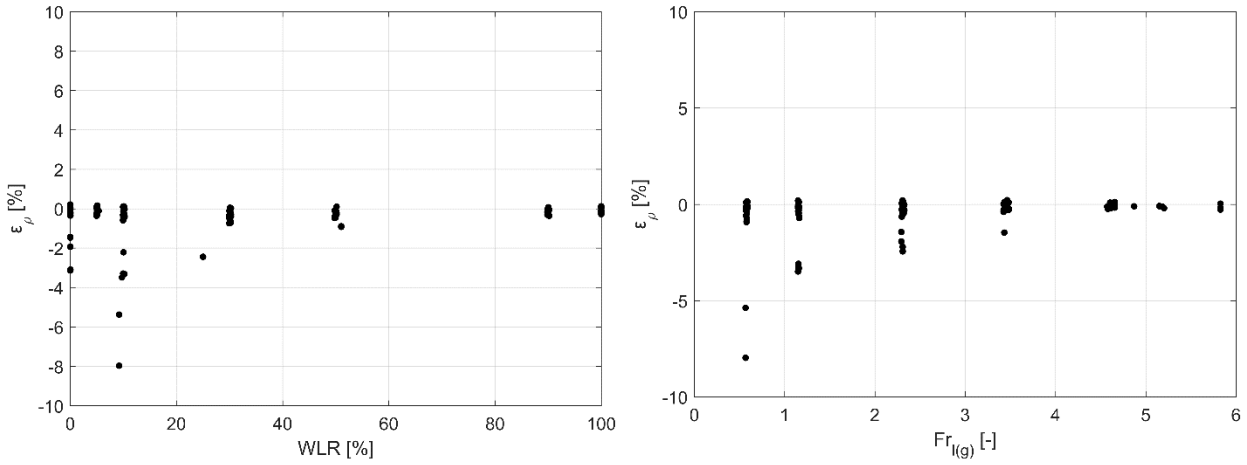

Figure 4-3 : Density error for oil-water mixtures as a function WLR (left) and $\mathrm{Fr}_{l(g)}$ (right) for Coriolis meters

4.1.3 Ultrasonic meters

Ultrasonic meters typically have issues with two phase oil-water flow in the dispersed regime. Small droplets will distort or attenuate the ultrasonic signal. In stratified oil-water flow they are able to measure in the different liquid layers and can measure the difference in speed of sound (SOS). The results of the liquid volumetric flow error as a function of WLR and $\mathrm{Fr}_{l(g)}$ are presented in Figure 4-4.

As observed from Figure 4-4, the error is much larger compared to the Coriolis data. At the pure oil and water boundary the majority of the data is observed, which means that in the interior domain (so for $0<\mathrm{WLR}<1$) more data was labelled invalid by the manufacturers. Again, minor degassing of the oil phase may be present at low WLR, however, the observed large error cannot be explained by the small amount of flashed gas from the oil (typically $\mathrm{GVF}<<1\%$).

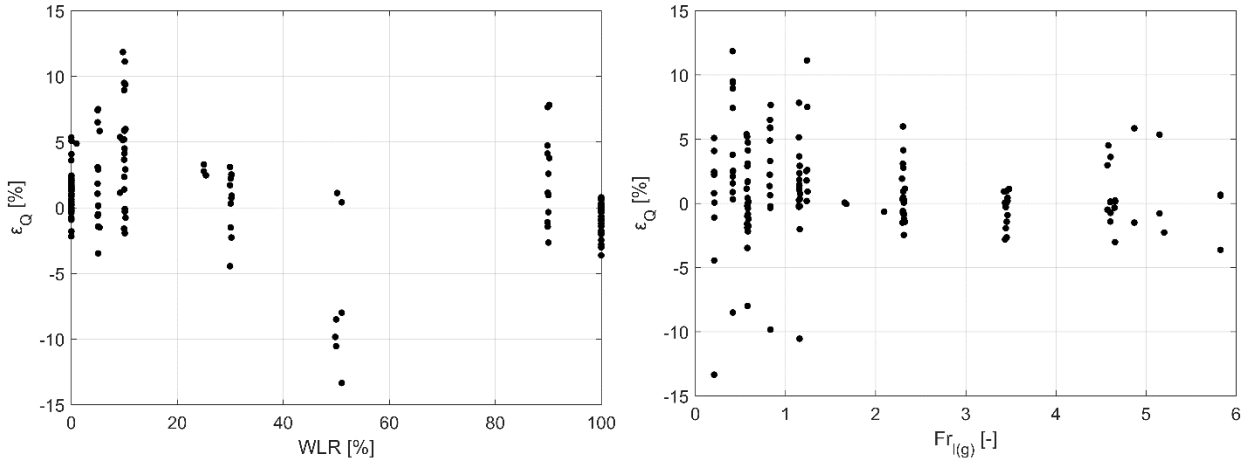

Figure 4-4 : Volumetric flow error for oil-water mixtures as a function WLR (left) and $\mathrm{Fr}_{l(g)}$ (right) for all ultrasonic meters

4.2 Oil-water mixtures with gas entrainment

In this section, the liquid test results with gas entrainment are presented. The deviation of the meters will be presented in terms of the "over-reading" for simplicity, even though the deviation may formally be an under-reading. The over-reading is based on the total liquid volume flow (ultrasonic) and total liquid mass flow (Coriolis). For the condition tested in this JTP, the difference between total mass flow and total liquid mass flow is negligible due to the low gas volume fractions and low gas densities.

4.2.1 Flow regimes

The over-reading will be a strong function of the type of flow regime. The observed flow regimes in the 4" line for several $\mathrm{Fr}_{l(g)}$ and $\mathrm{X}_{\mathrm{LM},l(g)} = 0.01$ are presented in Figure 4-5. The figure labels (a), (b) and (c) will be used in the subsequent figures to connect the $\mathrm{Fr}_{l(g)}$ dependence of the flow regime to the obtained measurement results. Figure 4-5 (a) and (d) provide the result for a stratified flow for $\mathrm{X}_{\mathrm{LM},l(g)} = 0.01$ and $\mathrm{X}_{\mathrm{LM},l(g)} = 0.03$, respectively, to illustrate the dependence of the gas hold-up on $\mathrm{X}_{\mathrm{LM},l(g)}$. As observed in these figures the gas-oil interface goes down as the $\mathrm{X}_{\mathrm{LM},l(g)}$ is increased, which is a direct measure for the gas hold-up. At high liquid flow rates the flow becomes almost opaque and the flash duration should be short to obtain a static picture of the multiphase flow. Therefore, at these conditions only gas-water or gas-oil photos are possible with low gas fractions.

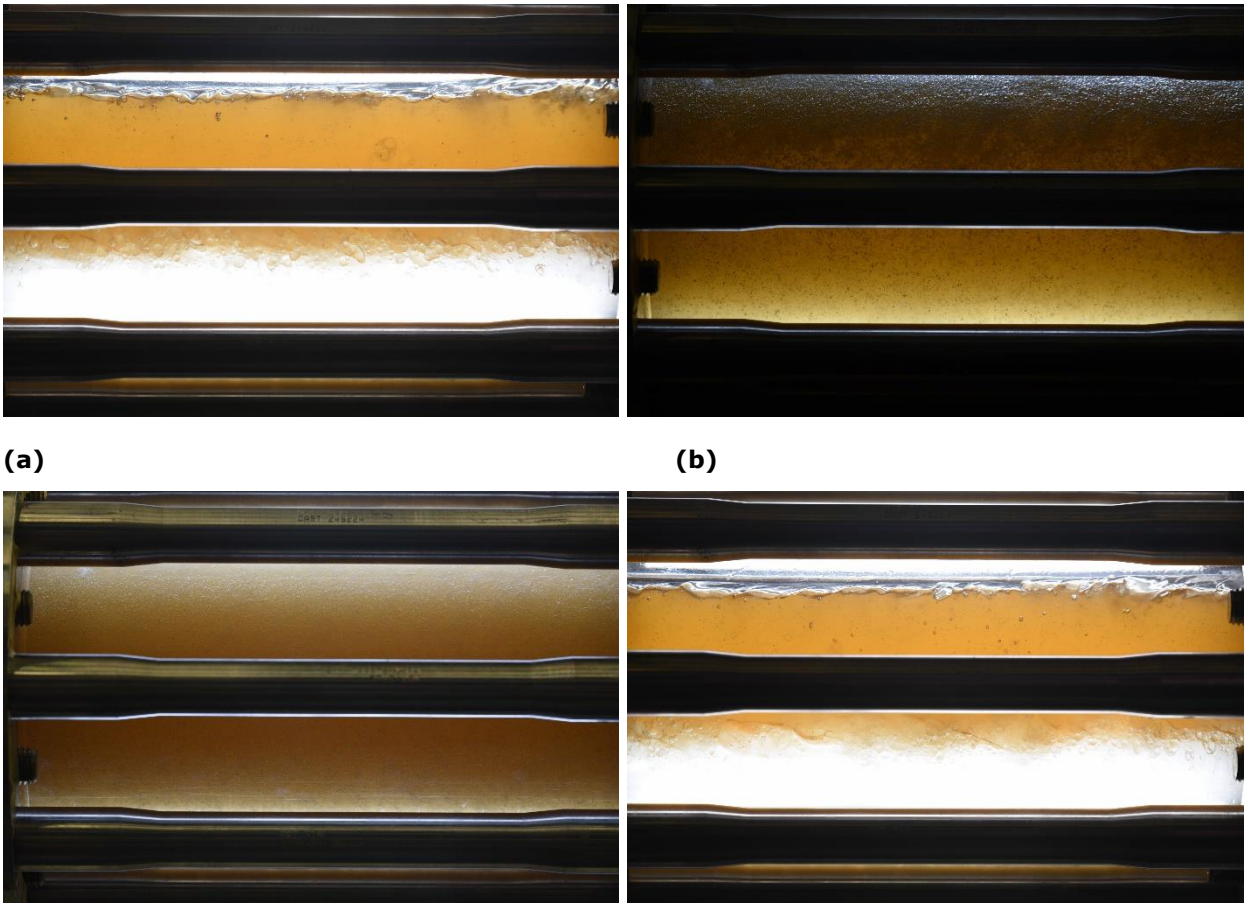

(a) **(b)**

(c) **(d)**

Figure 4-5 : Observed flow regimes for gas-oil-water mixtures for: (a) $\mathrm{Fr}_{l(g)} = 1.2\ (u_{sl} = 1.1)$ **,** $\mathrm{WLR} = 0.25$ **and** $\mathrm{X}_{\mathrm{LM},l(g)} = 0.01$**, (b)** $\mathrm{Fr}_{l(g)} = 2.4\ (u_{sl} = 2.3)$**,** $\mathrm{WLR} = 0$ **and** $\mathrm{X}_{\mathrm{LM},l(g)} = 0.01$**, (c)** $\mathrm{Fr}_{l(g)} = 4.8\ (u_{sl} = 4.5)$**,** $\mathrm{WLR} = 0$ **and** $\mathrm{X}_{\mathrm{LM},l(g)} = 0.005$**, (d)** $\mathrm{Fr}_{l(g)} = 1.2\ (u_{sl} = 1.1)$**,** $\mathrm{WLR} = 0.25$ **and** $\mathrm{X}_{\mathrm{LM},l(g)} = 0.03$**.**

4.2.2 Coriolis mass flow over-reading

The over-reading is based on mass flow rates and is defined as:

$$\mathrm{OR} = \frac{\dot{m}_l^{MUT}}{\dot{m}_l^{ref}}, \tag{15}$$

where $\dot{m}_l^{MUT}$ is the measured liquid mass flow rate by the MUT and $\dot{m}_l^{ref}$ is the liquid mass flow rate given by the reference system of the test facility, both at line conditions. In Figure 4-6, the over-reading of all Coriolis meters is plotted as a function of $\mathrm{X}_{\mathrm{LM},l(g)}$ and $\mathrm{Fr}_{l(g)}$.

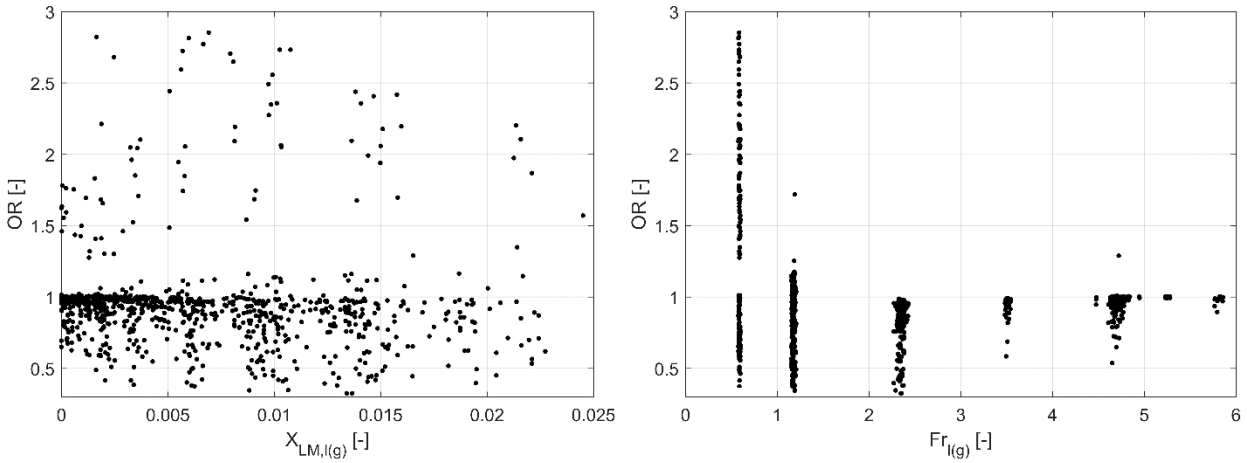

Figure 4-6 : Projection of over-reading of Coriolis meters as a function $X_{LM,l(g)}$ (left) and $Fr_{l(g)}$ (right)

The over-reading behaviour of the different Coriolis meters is not similar. It is observed that the Coriolis meters do not perform consistent at low liquid flow rates. Even very large over-readings are observed at these conditions, while in general the Coriolis meters under-read. At $Fr_{l(g)} > 2.5$, the flow becomes more homogeneous and the meter behaviour becomes similar. This is approximately equal to the estimated transition point of the gas-liquid flow to dispersed flow in section 2.2 and was demonstrated in Figure 4-5 (b) and (c). The under-reading response at higher liquid velocities is different between meters which appears as a scatter in the right figures of Figure 4-6.

It can be concluded that the meters show similar behaviour and respond in the same way to changes in the flow regime. The level of over/under-reading is however different and may be contributed to the meter settings and configuration, e.g. tube frequency and tube geometry.

4.2.3 Coriolis density

The "error" of the different Coriolis meters for the density measurement is given in Figure 4-7. In the determination of the error, it is assumed that the flow is homogeneous. Indeed, at high $Fr_{l(g)}$ this is a valid assumption and the error decreases. At low values, however, the flow cannot be considered homogeneous and the difference between the density measurement and the calculated homogeneous density increases. It is noted that this is mainly a fluid dynamical effect due to slip between the phases, i.e. the gas void fraction (basis for the density measurement) is not equal to the gas volume fraction (basis for the homogeneous density calculation of the reference system). Therefore, the error cannot be directly attributed to the Coriolis meters. This is strengthened by the fact that the behaviour between the different Coriolis meters is very consistent and the resulting errors are comparable.

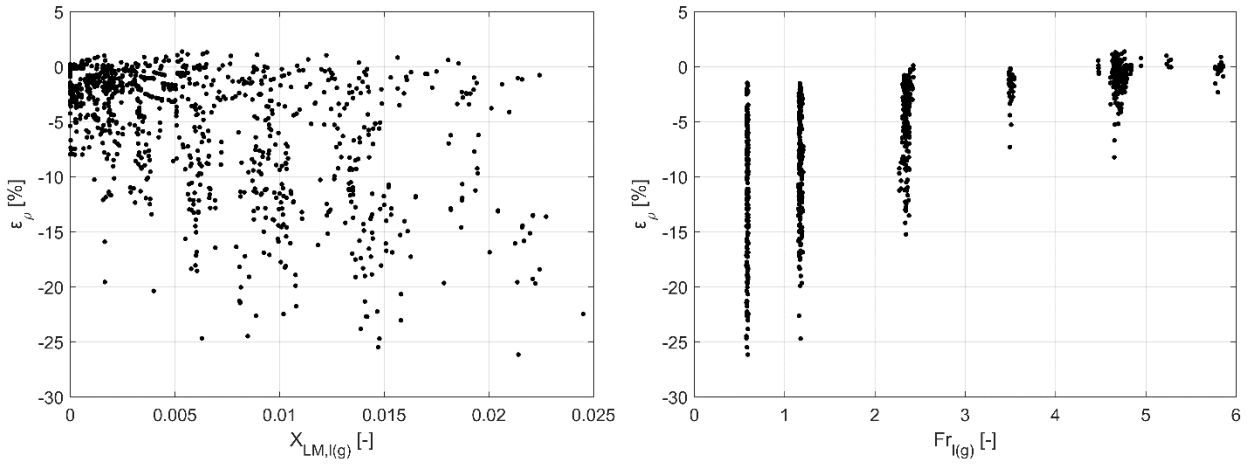

Figure 4-7 : Density measurement "error" of Coriolis meters as a function $\mathrm{X}_{\mathrm{LM}l(g)}$ (left) and $\mathrm{Fr}_{l(g)}$ (right)

4.2.4 Ultrasonic volumetric flow over-reading

The over-reading is based on volumetric flow rates and is defined as:

$$\mathrm{OR} = \frac{Q_l^{MUT}}{Q_l^{ref}}, \tag{16}$$

where Q_l^{MUT} is the measured total liquid volumetric flow rate by the MUT and Q_l^{ref} is the total liquid volumetric flow rate given by the reference system of the test facility, both at line conditions. In Figure 4-8, the over-reading of all ultrasonic meters is plotted as a function of $\mathrm{X}_{\mathrm{LM}l(g)}$ and $\mathrm{Fr}_{l(g)}$. It is noted that for the ultrasonic meters a large subset of the data produced volumetric flow rates of zero due to absence of a proper measurement, e.g. due to full attenuation of the ultrasonic signal. This flow conditions occurs at high $\mathrm{Fr}_{l(g)}$ and $\mathrm{X}_{\mathrm{LM}l(g)}$, which is also observed in Figure 4-8 when considering the number of valid test points in that region.

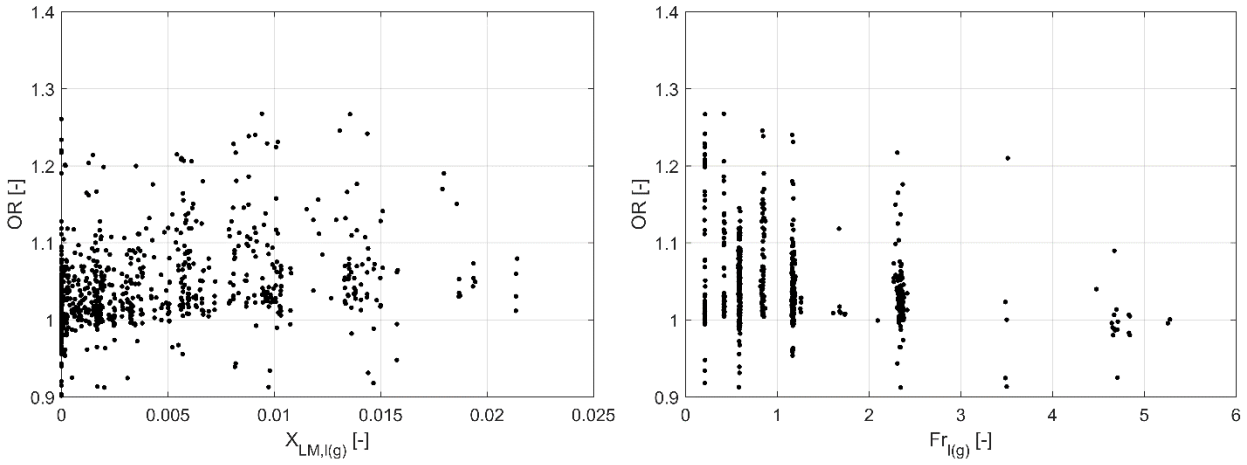

Figure 4-8 : Projection of over-reading of ultrasonic meters as a function $X_{LM,l(g)}$ (left) and $Fr_{l(g)}$ (right)

The over-reading has a clear systematic dependence on $X_{LM,l(g)}$ and $Fr_{l(g)}$. In the stratified regime, the over-reading is almost linear with $X_{LM,l(g)}$ and leads to a maximum over-reading of about 10%, which is small compared to typical wet gas over-readings. The over-reading decreases as the $Fr_{l(g)}$ increases. This can be explained by the larger slip velocity between the gas and liquid in stratified conditions which evidently results in a large gas hold-up. The multi-path ultrasonic meters perform path substitution. This means that the path location in e.g. the upper half-plane of the pipe (where the measurement is distorted by the gas), is substituted by the measurement of the velocity at the corresponding path in the lower half-plane of the pipe. Therefore, these meters are configured such that they do not compensate for the gas hold-up.

The over-reading decreases with $Fr_{l(g)}$ and seems to vanish at higher values. This conclusion cannot be safely drawn, however, since the data is only for low $X_{LM,l(g)}$ and at higher values the meters fail to measure, as observed in Figure 4-8.

In general, it seems that the ultrasonic meters can perform consistent in degassing oil-water flow as long as a measurement is established. Also, for consistent results it is necessary that all meters handle a path failure in the same way. For a range of path configurations, this means that path substitution should be applied.

5 CONCLUSIONS

DNV GL has executed a Joint Testing Project on the response of Coriolis and ultrasonic flow meters in phase contaminated oil flows. The aim of the project was to gain knowledge on the response of these flow meters to oil flow conditions with water contamination and minor gas contamination. To evaluate the performance of these meters, multiple meters from different manufacturers were installed to observe differences between meter designs.

During the JTP test, all possible flow regimes were covered for both the oil-water mixtures as well as the oil-water-gas mixtures. A dimensional analysis on the fundamental fluid dynamic equations of a multiphase flow was carried out which provided the dominant dimensionless numbers: the liquid Froude number, $\mathrm{Fr}_{l(g)}$, and the inverse Lockhart-Martinelli parameter, $\mathrm{X}_{\mathrm{LM}l(g)}$. The $\mathrm{Fr}_{l(g)}$ dominates the transition between stratified and dispersed flow and the $\mathrm{X}_{\mathrm{LM}l(g)}$ is the measure for the gas volume fraction, i.e. the level of gas contamination. At sufficiently high liquid velocities, i.e. high $\mathrm{Fr}_{l(g)}$, the oil-water flow will become disperse and can be considered as a homogeneous liquid. The same accounts for the gas-liquid mixture. These transition points were theoretically derived and confirmed by visual observations of the flow regimes during the performed experiments. The $\mathrm{X}_{\mathrm{LM}l(g)}$ strongly determined the over/under-reading of the flow meters.

The multiphase flow results of the Coriolis meters showed consistent behaviour and responded in the same way to changes in the flow regime. The level of over/under-reading was however different and could be contributed to the meter settings/configuration, e.g. tube frequency and geometry. Especially, the behaviour as a function of $\mathrm{Fr}_{l(g)}$ was very consistent and, at the conditions where the flow could be considered as homogeneous, the meters produced practically the same under-reading. At stratified conditions the meters diverged and very large difference were observed. Care needs to be taken when assessing the density measurement of a Coriolis meter. The density reference provided by a multiphase flow facility will typically assume a homogeneous mixture, which at low liquid Froude numbers will lose its validity.

Larger differences were observed for the ultrasonic meters. Generally, the ultrasonic meters produced valid results for low $\mathrm{Fr}_{l(g)}$ when the flow was still largely stratified. For these flow conditions the over-reading is systematic and limited to about 10% for the maximum tested gas fraction in the JTP. The meters failed when the multiphase flow (both two-phase oil-water and multiphase) became dispersed and the ultrasonic signal was fully attenuated by the flow.

6 REFERENCES

[1] P. Angeli and G.F. Hewitt, Flow structure in horizontal oil-water flow. *Int. J. Multiphase Flow* 26: 1117-1140 (2000).

[2] C.E. Brennen, *Fundamentals of Multiphase Flow* (Cambridge University Press, New York, 2005).

[3] E. Buckingham, On physically similar systems; illustrations of the use of dimensional equations. *Phys. Rev.* 4:345–376 (1914).

[4] G. Elseth, *An Experimental Study of Oil/Water Flow in Horizontal Pipes.* PhD-Thesis NTNU (2001).

[5] M. Ishii, *Thermo-fluid dynamic theory of two-phase flow* (Springer Verlag, Berlin, 2011).

[6] L.E. Kinsler, A.R. Frey, A.B. Coppens and J.V. Sanders, *Fundamentals of Acoustics* (John Wiley & Sons, New York, 2000); P.J. van Dijk, Acoustics in Two-Phase Pipe Flows. PhD-Thesis University Twente (2005).

[7] G. Meng, A. Jaworski and N.M. White, Composition measurements of crude oil and process water emulsions using thick-film ultrasonic transducers. *Chem. Eng. Process.* 45:383-391 (2006); R.J. Ulrick, A sound velocity method for determining the compressibility of finely divided substances, *J. Appl. Phys.* 18:983-987 (1947).

[8] D.S. van Putten, *Flow Rate Reconstruction and Uncertainty Model of the MultiPhase Flow Facility Groningen*, GCS-2013-2111C (2014).

[9] D.S. van Putten *et al.*, Ultrasonic meters in wet gas applications, North Sea Flow Measurement Workshop, paper 1.2 (2015).

[10] Y Taitel and A.E. Dukler, A Model for Predicting Flow Regime Transitions in Horizontal and Near Horizontal Gas-Liquid Flow. *AIChE Journal* 20:47–55 (1976).

[11] J.A. Weinstein, D.R. Kassoy and M.J. Bell, Experimental study of oscillatory motion of particles and bubbles with application to Coriolis flow meters, *Phys. Fluids* 20:103306 (2008)

[12] J. Weisman, D. Duncan, J. Gibson and T. Crawford, Effects of fluid properties and pipe diameter on two-phase flow patterns in horizontal lines. *Int. J. Multiphase Flow* 5:437–462 (1979).